Journal of Sound and Vibration (2003) **259**(4), 809–828
doi:10.1006/jsvi.2002.5123, available online at http://www.idealibrary.com on IDEAL®

FREQUENCY RESPONSE OF A MODERATELY THICK ANTISYMMETRIC CROSS-PLY CYLINDRICAL PANEL USING MIXED TYPE OF FOURIER SOLUTION FUNCTIONS

H. R. H. KABIR

Engineering & Analysis Division, NASA Kennedy Space Center, Cape Canaveral, FL, U.S.A.

A. M. AL-KHALEEFI

Department of Civil Engineering, Kuwait University P.O. Box 5969, *Safat* 13060, *Kuwait*

AND

R. A. CHAUDHURI

Department of Materials Science and Engineering University of Utah, Salt Lake City, UT, U.S.A.
E-mail: r.chaudhuri@m.cc.utah.edu

(*Received* 14 *June* 2001, *and in final form* 1 *March* 2002)

A hitherto unavailable analytical solution to the boundary-value problem of the free vibration response of shear-flexible antisymmetric cross-ply laminated cylindrical panels is presented. The laminated shell theory formulation is based on the first order shear deformation theory (FSDT) including rotatory and surface-parallel inertias. The governing equations of the panel are defined by five highly coupled partial differential equations in five unknowns—three displacements, and two rotations. The assumed solution functions for the eigen/boundary-value problem are selected in terms of mixed-type double Fourier series. Numerical results presented for parametric effects, such as length-to-thickness ratio and radius-to-thickness ratio, should serve as a bench mark for future comparison. A four-node shear-flexible finite element is selected to compare the results with the present solution.

1. INTRODUCTION

Free vibration response analysis of laminated circular cylindrical panels (open shallow shells used in aircraft fuselages, wings, boats, etc.), fabricated with fiber-reinforced laminated composite materials such as glass/epoxy, graphite/epoxy, graphite/graphite, boron/epoxy, Kevlar-49/epoxy, etc., are of current interest because of their increasing use in aerospace, hydrospace, energy, chemical, and other industrial applications [1]. A variety of factors, such as high strength-to-weight and stiffness-to-weight ratios (resulting in fuel economy), corrosion resistance, longer fatigue life and stealth characteristics (of military aircraft, e.g., stealth fighter, F117A) are responsible for increased usage of fiber-reinforced composite laminates in aerospace structural applications. A more recent advancement in composites in the commercial aircraft sector, e.g., all-composite empennages on the Boeing 7J7 and Douglas MD-91X, is to limit sonic fatigue caused by the new fuel-efficient propfan or unducted fan

0022-460X/02/$35.00

(UDF) engines. All these advancements and design requirements place a premium on an in-depth understanding of the response characteristics of such structural components. The present study is intended to capture some of these intricacies of the dynamic response of laminated composite structural components through analysis of a model problem — a moderately thick antisymmetric cross-ply laminated cylindrical panel. Analysis of moderately thick panels are, in general, based on the first order shear deformation theory (FSDT).

Typically, laminated composite structures are analyzed using approximate numerical techniques, such as finite element methods (FEM) and boundary element methods (BEM), the accuracy of which is usually ascertained by comparing with certain bench-mark analytical (or strong form of) solutions. Derivation of analytical (e.g., Fourier series) solutions for the problems of laminated curved panels fabricated with such advanced composite materials as graphite/epoxy, boron/epoxy, graphite/PEEK, etc., is, however, fraught with some complexities, such as asymmetry of lamination (resulting in bending–stretching coupling), effect of transverse shear deformation (caused by low transverse shear modulus-to-surface-parallel Young's modulus ratio), and curvature effect. Additional complexities arise by way of satisfying boundary conditions, that cannot be handled by traditional analytical approaches, such as the almost two centuries-old Navier's and close to a century-old Levy's approaches [2].

A detailed review of the literature pertaining to the subject matter of the present study is already available in recent publications, e.g., references [3–11], and will not be repeated here in the interest of brevity of presentation. An in-depth review of this literature reveals that the solution to the problem of free vibration of antisymmetric cross-ply moderately thick cylindrically curved panels, with general type admissible boundary conditions prescribed at the edges, is still non-existent in the literature, which is the subject matter of the present investigation. Additionally, the boundary discontinuous double Fourier series technique employed so far in the analysis of cylindrical and doubly curved panels [4, 6, 8] is based on the approach due to Chaudhuri [2]. This approach recommends that the assumed solution for a cross-ply panel should require only a single set of Fourier series for each displacement and rotation component. It may be noted here that although Fourier series expansion is, in theory, a valid approach to derive the Green's function for a boundary-value problem, in practice, the convergence is not uniform and very slow because the Green's function has a singularity. For example, the Green's function for two-dimensional Laplace's equation has a logarithmic singularity, which obviously cannot be evaluated accurately enough by any reasonably small finite sum in the double Fourier series [12]. Acceleration of convergence has been a major theme of research during the last several decades, especially in the Russian literature on the subject [12]. The primary objective of the present investigation is to find a novel way to achieve this accelerated convergence, which has so far eluded researchers in this field. Inclusion of a second series, which is orthogonal to the first, in the assumed solution is a novel idea that is yet to be explored. Additionally, we have computed hitherto unavailable numerical results for an important laminated shell boundary-value problem. In what follows, the afore-mentioned novel idea is implemented in the investigation of the model problem pertaining to the frequency response of an antisymmetric cross-ply moderately thick cylindrical panel subjected to the SS2 (see, e.g., reference [8] for definition) type simply supported boundary condition in order to obtain a more rapid convergence.

2. BASIC EQUATIONS

A laminated cylindrical panel of total thickness, h, is shown in Figure 1. The thickness of the kth layer is denoted by $t^{(k)} = \alpha_3^k - \alpha_3^{k-1}$, in which $\alpha_3^{(k)}$ and $\alpha_3^{(k-1)}$, $k = 1, 2, \ldots, N$, are

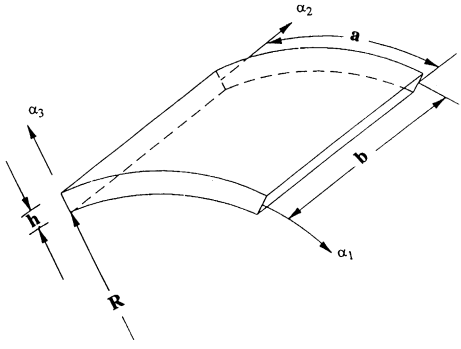

Figure 1. A typical cylindrical panel.

the distances from the reference surface to the outer and inner faces, respectively, of the layer measured from the mid-depth of the panel. An orthogonal curvilinear co-ordinate system is selected to define the geometry of the panel. The co-ordinate system is placed at the mid-height of the panel thickness. The curvilinear co-ordinates α_1, α_2 define the reference surface ($\alpha_3 = 0$) of the panel. The spans a and b are measured along the axes α_1 and α_2, respectively, while R denotes the radius of the reference surface (see Figure 1). The equations of motion, based on the Sanders [13] moderately deep shell theory, can be written as:

$$\frac{\partial N_1}{\partial \alpha_1} + \frac{\partial N_6}{\partial \alpha_2} + \frac{1}{2R}\frac{\partial M_6}{\partial \alpha_2} + \frac{Q_1}{R} = m_1, \tag{1a}$$

$$\frac{\partial N_6}{\partial \alpha_1} - \frac{1}{2R}\frac{\partial M_6}{\partial \alpha_1} + \frac{\partial N_2}{\partial \alpha_2} = m_2, \tag{1b}$$

$$\frac{\partial Q_1}{\partial \alpha_1} + \frac{\partial Q_2}{\partial \alpha_2} - \frac{N_1}{R} = m_3, \tag{1c}$$

$$\frac{\partial M_1}{\partial \alpha_1} + \frac{\partial M_6}{\partial \alpha_2} - Q_1 = m_4, \quad \frac{\partial M_6}{\partial \alpha_1} + \frac{\partial M_2}{\partial \alpha_2} - Q_2 = m_5, \tag{1d, e}$$

where N_1, N_2, and N_6 are the surface parallel stress resultants, while M_1, M_2 and M_6 are stress couples or moment resultants, and Q_1 and Q_2 represent the transverse shear stress resultants, all per unit length. The inertias m_i ($i = 1, \ldots, 5$) are defined as:

$$m_1 = \left(\rho_1 + \frac{2\rho_2}{R}\right)\frac{\partial^2 u_1}{\partial t^2} + \left(\rho_2 + \frac{2\rho_3}{R}\right)\frac{\partial^2 \phi_1}{\partial t^2}, \tag{2a}$$

$$m_2 = \rho_1 \frac{\partial^2 u_2}{\partial t^2} + \rho_2 \frac{\partial^2 \phi_2}{\partial t^2}, \quad m_3 = \rho_1 \frac{\partial^2 u_3}{\partial t^2}, \tag{2b, c}$$

$$m_4 = \left(\rho_2 + \frac{\rho_3}{R}\right)\frac{\partial^2 u_2}{\partial t^2} + \rho_3 \frac{\partial^2 \phi_1}{\partial t^2}, \quad m_5 = \rho_2 \frac{\partial^2 u_2}{\partial t^2} + \rho_3 \frac{\partial^2 \phi_2}{\partial t^2}, \tag{2d, e}$$

in which both the surface-parallel and rotatory inertias are included. u_i ($i = 1, 2, 3$) represents the displacement components at the reference surface along α_i ($i = 1, 2, 3$) axes, while ϕ_i ($i = 1, 2$) refers to rotations of the normal about α_i ($i = 1, 2$) axes. Finally, the

weighted averaged density ρ_i ($i=1, 2, 3$) is defined as

$$(\rho_1, \rho_2, \rho_3) = \sum_{k=1}^{N} \int_{\alpha_3^{(k-1)}}^{\alpha_3^{(k)}} \rho^{(k)}(1, \alpha_3, \alpha_3^2)\, \mathrm{d}\alpha_3, \tag{3}$$

where $\rho^{(k)}$ and N represent the density of the kth layer material, and the total number of layers respectively. For a general cross-ply laminated panel, surface-parallel stress resultants, N_i, $i=1, 2, 6$, stress couples, M_i, $i=1, 2, 6$, and the transverse shear stress resultants, Q_i, $i=1, 2$, are related to the mid-surface strains, ε_i^0, and changes of curvature and twist, κ_i, by

$$N_i = A_{ij}\varepsilon_j^0 + B_{ij}\kappa_i, \quad (i, j = 1, 2), \tag{4a}$$

$$N_6 = A_{66}\varepsilon_6^0 + B_{66}\kappa_6, \tag{4b}$$

$$M_i = B_{ij}\varepsilon_j^0 + D_{ij}\kappa_j, \quad (i,j = 1, 2), \tag{4c}$$

$$M_6 = B_{66}\kappa_6 + D_{66}\kappa_6, \tag{4d}$$

$$Q_1 = A_{55}\varepsilon_5^0, \quad Q_2 = A_{44}\varepsilon_4^0, \tag{4e, f}$$

with

$$A_{55} = K_1^2 A_{55}^*, \quad A_{44} = K_2^2 A_{44}^*, \tag{5}$$

where A_{ij}, B_{ij}, and D_{ij}, $i, j=1, 2, 6$, are extensional, coupling, and bending rigidities respectively. A_{44}^* and A_{55}^* represent transverse shear rigidities, while K_1^2 and K_2^2 are shear correction factors ε_j^0 ($j=1, 2, 4, 5, 6$) and κ_j ($j=1, 2, 6$) are related to displacement components and their derivatives, as defined by Sanders [12], and are given as

$$\varepsilon_1^0 = u_{1,1} + \frac{u_3}{R_1}, \quad \varepsilon_2^0 = u_{2,2}, \tag{6a, b}$$

$$\varepsilon_4^0 = u_{3,2} + \phi_2, \quad \varepsilon_5^0 = u_{3,1} + \phi_1, \quad \varepsilon_6^0 = u_{2,1} + u_{1,2}, \tag{6c–e}$$

$$\kappa_1 = \phi_{1,1}, \quad \kappa_2 = \phi_{2,2}, \quad \kappa_6 = \phi_{2,1} + \phi_{1,2} + \frac{1}{2R}(u_{2,1} - u_{1,2}). \tag{6f–h}$$

Substitution of equations (4)–(6) into equations (1) yields five highly coupled partial differential equations with constant coefficients. These equations can be written in a differential operator matrix form as

$$\mathbf{Tv} = \mathbf{f}, \tag{7}$$

where

$$T_{ij} = T_{ji}, \quad i, j = 1, \ldots, 5, \tag{8a}$$

$$\mathbf{v}^{\mathrm{T}} = \{u_1, u_2, u_3, \phi_1, \phi_2\}, \quad \mathbf{f}^{\mathrm{T}} = \{m_1, m_2, m_3, m_4, m_5\}. \tag{8b, c}$$

The components of the differential operator T_{ij} can be written as:

$$T_{11} = -\frac{A_{55}}{R^2}(\,) + A_{12}(\,)_{,\alpha_1\alpha_1} + \left(A_{66} + \frac{2}{R}B_{66} + \frac{1}{R^2}D_{66}\right)(\,)_{,\alpha_2\alpha_2}, \tag{9a}$$

$$T_{12} = \left(A_{12} + A_{66} - \frac{1}{R^2}D_{66}\right)(\,)_{,\alpha_1\alpha_2}, \tag{9b}$$

$$T_{13} = \left(\frac{A_{11}}{R} + \frac{A_{55}}{R}\right)(\,)_{,\alpha_1\alpha_2}, \tag{9c}$$

$$T_{14} = -\frac{A_{55}}{R}(\,) + B_{11}(\,)_{,\alpha_1\alpha_1} + \left(B_{66} + \frac{1}{R}D_{66}\right)(\,)_{,\alpha_1\alpha_2}, \tag{9d}$$

$$T_{15} = \left(B_{12} + B_{66} - \frac{1}{R}D_{66}\right)(\,)_{,\alpha_1\alpha_2}, \tag{9e}$$

$$T_{22} = \left(A_{66} - \frac{2}{R}B_{66} + \frac{1}{R^2}D_{66}\right)(\,)_{,\alpha_1\alpha_2}, \tag{9f}$$

$$T_{23} = \frac{A_{12}}{R}(\,)_{,\alpha_2}, \quad T_{24} = \left(B_{12} + B_{66} - \frac{1}{R}D_{66}\right)(\,)_{,\alpha_1\alpha_2}, \tag{9g, h}$$

$$T_{25} = \left(B_{66} - \frac{1}{R}D_{66}\right)(\,)_{,\alpha_1\alpha_2}, \tag{9i}$$

$$T_{33} = \frac{A_{11}}{R^2}(\,) + A_{55}(\,)_{,\alpha_1\alpha_2} + A_{44}(\,)_{,\alpha_2\alpha_2}, \tag{9j}$$

$$T_{34} = \left(A_{55} - \frac{B_{11}}{R}\right)(\,)_{,\alpha_1}, \quad T_{35} = \left(A_{44} - \frac{B_{12}}{R}\right)(\,)_{,\alpha_2}, \tag{9k, l}$$

$$T_{44} = A_{55}(\,) + D_{11}(\,)_{,\alpha_1\alpha_1} + D_{66}(\,)_{,\alpha_2\alpha_2}, \tag{9m}$$

$$T_{45} = (D_{12} + D_{66})(\,)_{,\alpha_1\alpha_2}, \tag{9n}$$

$$T_{55} = -A_{44}(\,) + D_{66}(\,)_{,\alpha_1\alpha_1} + D_{22}(\,)_{,\alpha_2\alpha_2}. \tag{9o}$$

An admissible simply supported boundary condition, generally referred to as SS2 [8], is chosen to illustrate the present solution procedure. This is of the following form:

$$u_n = N_t = u_3 = M_n = \phi_t = 0, \tag{10a–e}$$

where, n and t denote normal and tangential components of displacement, stress resultant and stress couple vectors in reference to the edges [8] respectively. The main objective here is to solve the system of partial differential equations, given by equations (7)–(9) subjected to the boundary conditions, given by equations (10).

3. SOLUTION TO THE BOUNDARY-VALUE PROBLEM

The assumed solution functions for the boundary-value problem of a finite dimensional cross-ply laminated cylindrical panel are selected in terms of double Fourier series in the

following form:

$$u_1(\alpha_1, \alpha_2, t) = \sum_{m=0}^{\infty}\sum_{n=1}^{\infty} {}^1C^{\mathrm{I}}_{mn} \cos\left(\frac{m\pi\alpha_1}{a}\right) \sin\left(\frac{m\pi\alpha_2}{b}\right) e^{i\omega t} + \sum_{m=0}^{\infty}\sum_{n=1}^{\infty} {}^2C^{\mathrm{I}}_{mn} \sin\left(\frac{m\pi\alpha_1}{a}\right) \cos\left(\frac{m\pi\alpha_2}{b}\right) e^{i\omega t}, \tag{11a}$$

$$u_2(\alpha_1, \alpha_2, t) = \sum_{m=0}^{\infty}\sum_{n=1}^{\infty} {}^1C^{\mathrm{II}}_{mn} \sin\left(\frac{m\pi\alpha_1}{a}\right) \cos\left(\frac{m\pi\alpha_2}{b}\right) e^{i\omega t} + \sum_{m=0}^{\infty}\sum_{n=1}^{\infty} {}^2C^{\mathrm{II}}_{mn} \cos\left(\frac{m\pi\alpha_1}{a}\right) \sin\left(\frac{m\pi\alpha_2}{b}\right) e^{i\omega t}, \tag{11b}$$

$$u_3(\alpha_1, \alpha_2, t) = \sum_{m=1}^{\infty}\sum_{n=1}^{\infty} {}^1C^{\mathrm{III}}_{mn} \sin\left(\frac{m\pi\alpha_1}{a}\right) \sin\left(\frac{m\pi\alpha_2}{b}\right) e^{i\omega t} + \sum_{m=0}^{\infty}\sum_{n=0}^{\infty} {}^2C^{\mathrm{III}}_{mn} \cos\left(\frac{m\pi\alpha_1}{a}\right) \cos\left(\frac{m\pi\alpha_2}{b}\right) e^{i\omega t}, \tag{11c}$$

$$\phi_1(\alpha_1, \alpha_2, t) = \sum_{m=0}^{\infty}\sum_{n=1}^{\infty} {}^1C^{\mathrm{IV}}_{mn} \cos\left(\frac{m\pi\alpha_1}{a}\right) \sin\left(\frac{m\pi\alpha_2}{b}\right) e^{i\omega t} + \sum_{m=1}^{\infty}\sum_{n=0}^{\infty} {}^2C^{\mathrm{IV}}_{mn} \sin\left(\frac{m\pi\alpha_1}{a}\right) \cos\left(\frac{m\pi\alpha_2}{b}\right) e^{i\omega t}, \tag{11d}$$

$$\phi_2(\alpha_1, \alpha_2, t) = \sum_{m=1}^{\infty}\sum_{n=0}^{\infty} {}^1C^{\mathrm{V}}_{mn} \sin\left(\frac{m\pi\alpha_1}{a}\right) \cos\left(\frac{m\pi\alpha_2}{b}\right) e^{i\omega t} + \sum_{m=0}^{\infty}\sum_{n=1}^{\infty} {}^2C^{\mathrm{V}}_{mn} \cos\left(\frac{m\pi\alpha_1}{a}\right) \sin\left(\frac{m\pi\alpha_2}{b}\right) e^{i\omega t}, \tag{11e}$$

where ${}^jC^i_{mn}$ ($i = \mathrm{I}, \ldots, \mathrm{V}$; $j = 1, \ldots, 2$) represents the Fourier coefficients.

It is quite interesting to note that the first of each set of assumed solution functions in equations (11) is sufficient for solving the boundary-value problem under investigation [2, 8]. However, it is well known from the theory of Fourier series that the rate of convergence becomes less rapid in the presence of discontinuities in the function or its first (normal) derivative. In order to alleviate this difficulty, each unknown is expressed in terms of two double Fourier series in which the second set is orthogonal to the first, and represents the error term that may arise out of the presence of discontinuity in the function or its first derivative at the boundary. This is believed to produce accelerated convergence of the series solution.

In order to illustrate the above, the assumed solution function for u_1 is considered:

$$u_1(\alpha_1, \alpha_2, t) = {}^1u_1(\alpha_1, \alpha_2, t) + {}^2u_1(\alpha_1, \alpha_2, t), \tag{12}$$

where

$${}^1u_1(\alpha_1, \alpha_2, t) = \sum_{m=0}^{\infty}\sum_{n=1}^{\infty} {}^1C^{\mathrm{I}}_{mn} \cos\left(\frac{m\pi\alpha_1}{a}\right) \sin\left(\frac{m\pi\alpha_2}{b}\right) e^{i\omega t}, \quad \text{not valid at } \partial\Omega \tag{13a}$$

and

$$^{2}u_1(\alpha_1,\ \alpha_2,\ t) = \sum_{m=1}^{\infty}\sum_{n=0}^{\infty} {}^{2}C^{\mathrm{I}}_{mn}\sin\left(\frac{m\pi\alpha_1}{a}\right)\cos\left(\frac{m\pi\alpha_2}{b}\right)\mathrm{e}^{\mathrm{i}\omega t} \quad \text{valid at } \partial\Omega, \tag{13b}$$

where $\partial\Omega$ represents the boundaries.

Since $^{1}u_1(\alpha_1,\ \alpha_2,\ t)$, given by equation (13a), does not satisfy the boundary conditions at $\alpha_1 = (0,\ a)$, it is forced to satisfy these, which results in $2n$ algebraic equations:

$$\sum_{m=1}^{\infty} W_m^{(1)}\,{}^{1}C^{\mathrm{I}}_{mn} = 0, \quad {}^{1}C^{\mathrm{I}}_{0n} + \sum_{m=1}^{\infty} W_m^{(2)}\,{}^{1}C^{\mathrm{I}}_{mn} = 0, \tag{14a, b}$$

where $W_m^{(1)}$ and $W_m^{(2)}$ are defined as

$$\left(W_m^{(1)},\ W_m^{(2)}\right) = \begin{cases} (0,\ 1), & m = \text{odd}, \\ (1,\ 0), & m = \text{even}. \end{cases} \tag{15}$$

The above operation paves the way for term-by-term differentiation. Therefore,

$$^{1}u_{1,1}(\alpha_1,\ \alpha_2,\ t) = -\sum_{m=1}^{\infty}\sum_{n=1}^{\infty}\frac{m\pi}{a}\,{}^{1}\mathrm{C}^{\mathrm{I}}_{mn}\sin\left(\frac{m\pi\alpha_1}{a}\right)\sin\left(\frac{m\pi\alpha_2}{b}\right)\mathrm{e}^{\mathrm{i}\omega t}, \quad 0<\alpha_1<a, \quad 0<\alpha_2<b. \tag{16}$$

Further term-by-term differentiation is, however, not possible due to the presence of discontinuity at the boundaries at $\alpha_1 = (0,\ a)$. $^{1}u_{1,11}$ is then expanded in the following form:

$$\begin{aligned} {}^{1}u_{1,1\ 1}(\alpha_1,\ \alpha_2,\ t) = &\frac{1}{2}\sum_{n=1}^{\infty}\left[a^{1111}_{n(1)}\sin\left(\frac{n\pi\alpha_2}{b}\right)\mathrm{e}^{i\omega t}\right. \\ &\left.+\sum_{m=1}^{\infty}\sum_{n=1}^{\infty}\left\{\frac{m^2\pi^2}{a^2}\,{}^{1}C^{\mathrm{I}}_{mn} + W_m^{(1)}a^{1111}_{n(1)} + W_m^{(2)}a^{1111}_{n(2)}\right\}\cos\left(\frac{m\pi\alpha_1}{a}\right)\sin\left(\frac{m\pi\alpha_2}{b}\right)\mathrm{e}^{\mathrm{i}\omega t}. \right. \end{aligned} \tag{17}$$

The above operation gives rise to two unknown boundary Fourier coefficients $a^{1111}_{n(1)}$ and $a^{1111}_{n(2)}$ defined as

$$a^{1111}_{n(1)} = \frac{4}{ab}\int_0^a \left[{}^{1}u_{1,1}(a,\ \alpha_2,\ t) - {}^{1}u_{1,1}(0,\ \alpha_2,\ t)\right]\sin\left(\frac{m\pi\alpha_2}{b}\right)\mathrm{d}\alpha_2, \tag{18a}$$

$$a^{1111}_{n(2)} = -\frac{4}{ab}\int_0^a \left[{}^{1}u_{1,1}(a,\ \alpha_2,\ t) + {}^{1}u_{1,1}(0,\ \alpha_2,\ t)\right]\sin\left(\frac{m\pi\alpha_2}{b}\right)\mathrm{d}\alpha_2. \tag{18b}$$

Substitution of the assumed functions and their derivatives into the governing system of partial differential equations, given by equations (7–9) and boundary conditions, given by equation (10) finally yields, on equating the coefficients of $\cos(\alpha_m x_1)\sin(\beta_n x_2)$, $\sin(\alpha_m x_1)\cos(\beta_n x_2)$, etc., $10mn + 5m + 5n + 1$ simultaneous linear algebraic equations. The details of this procedure, which is illustrated elsewhere for the static case (see, e.g., references [4, 6, 8]), are omitted here in the interest of brevity. The computation of the eigenvalues (natural frequencies) is carried out utilizing the standard library of IMSL software [14].

4. NUMERICAL RESULTS AND DISCUSSION

In what follows, a two-layer [0°/90°] laminated cylindrical panel of square planform is numerically investigated. Each of the laminae is assumed to be of the same thickness. A computer program is developed to solve the eigenvalue problem described above. The mode shapes (eigenfunctions) are extracted and plotted using the routine, SURFER. The numerical results are obtained for the following boron/epoxy layer–material properties: $E_1/E_2 = 13{\cdot}818$, $G_{12}/E_2 = G_{13}/E_2 = 0{\cdot}418$, $G_{23}/E_2 = 0{\cdot}272$, $\nu_{12} = \nu_{13} = 0{\cdot}34$, $\nu_{23} = 0{\cdot}34$, $K_1^2 = K_2^2 = \frac{5}{6}$, where E_1 and E_2 are Young's moduli along major and minor axes, respectively, of a lamina. G_{12} is the surface-parallel shear modulus, while G_{13} and G_{23} are transverse shear moduli in the $\alpha_1-\alpha_3$ and $\alpha_2-\alpha_3$ planes respectively. ν_{ij} denote Poisson's ratios. The following normalized frequency term is defined for convenience:

$$\lambda_i = \omega_i a^2 \sqrt{(\rho/(10E_2))}/h, \quad i = 1, 2, 3, \ldots, \tag{19}$$

where ω_i, $i = 1, 2, 3, \ldots$, denotes the natural frequencies in numerical orders of magnitudes.

First, the accuracy of the present solution as applied to the antisymmetric cross-ply cylindrical panel boundary-value problem under consideration is numerically ascertained by studying the convergence characteristics of the computed natural frequencies (eigenvalues). Various parametric studies such as dependence on R/a, a/h and $m = n$ are performed, a sampling of which is exhibited here (others will be made available to interested readers upon request). Figures 2–4 present the lowest normalized natural frequencies for moderately deep ($R/a = 10$) cylindrical panels of square ($b/a = 1$) planform and $a/h = 10$, 20, 50 respectively. In each case, a rapid convergence is achieved at or before $m = n = 5$. The lower natural frequencies, e. g., the lowest four, converge more rapidly (at or before $m = n = 3$) than the higher ones, such as the fifth, sixth and seventh. Similar trend is also observed for much shallower ($R/a = 100$) square cylindrical panels as shown in Figures 5–7, the length-to-thickness ratios remaining the same as before. Convergence plots for virtually flat ($R/a = 1000$) antisymmetric cross-ply [0°/90°] cylindrical panels are not included here in the interest of brevity of presentation. It may be remarked that these results do not constitute a mathematically rigorous convergence proof, but merely

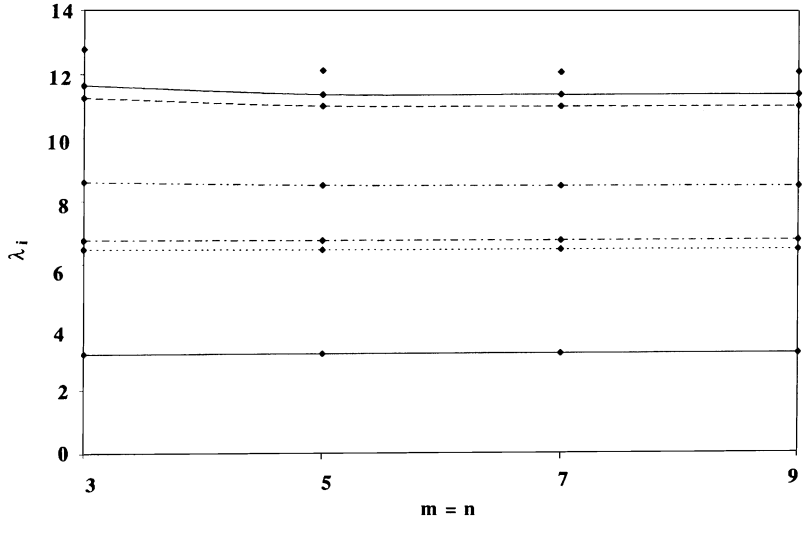

Figure 2. Convergence of seven lowest natural frequencies of a [0°/90°] moderately thick ($a/h = 10$), moderately deep ($R/a = 10$) square cylindrical panel.

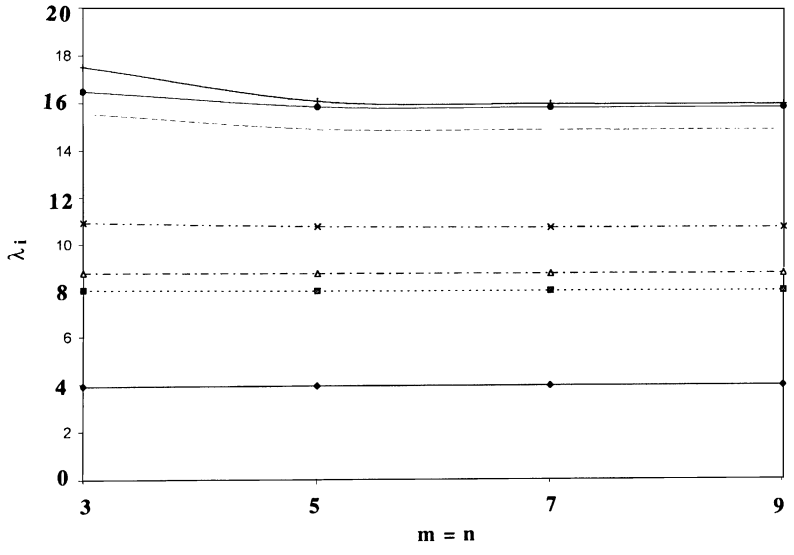

Figure 3. Convergence of seven lowest natural frequencies of a [0°/90°] moderately thick ($a/h = 20$), moderately deep ($R/a = 10$) square cylindrical panel.

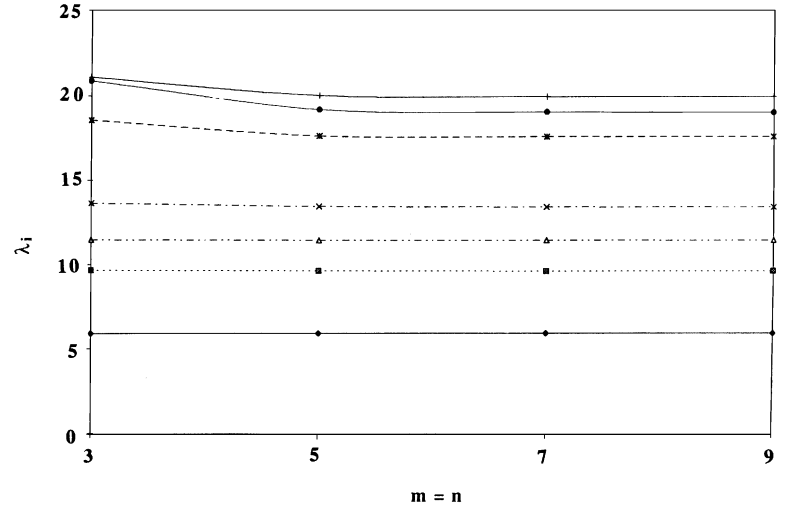

Figure 4. Convergence of seven lowest natural frequencies of a [0°/90°] thin ($a/h = 50$), moderately deep ($R/a = 10$) square cylindrical panel.

demonstrate satisfaction of the necessary (but not sufficient) condition for convergence, which is acceptable in the engineering literature.

Figures 8 and 9 numerically address the main innovation of the present investigation, which is concerned with the use of mixed type mutually orthogonal sets of double Fourier series. These plots present convergence results for the first five normalized natural frequencies of a [0°/90°] moderately thick ($a/h = 10$) very shallow ($R/a = 100$) square cylindrical panel, with and without the second set of double Fourier series. It may be noted

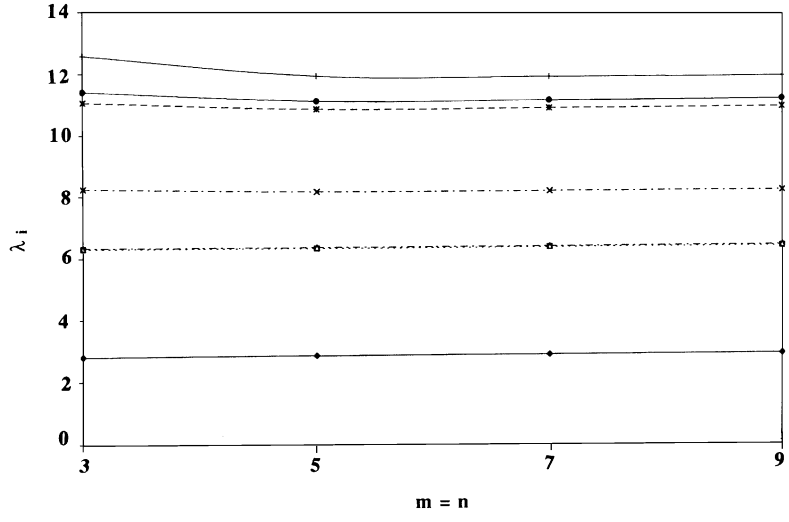

Figure 5. Convergence of seven lowest natural frequencies of a [0°/90°] moderately thick ($a/h=10$), very shallow ($R/a=100$) square cylindrical panel.

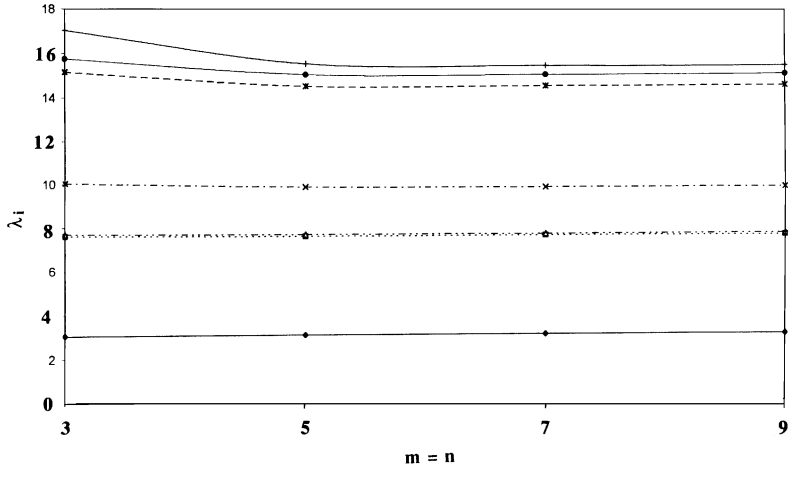

Figure 6. Convergence of seven lowest natural frequencies of a [0°/90°] moderately thick ($a/h=20$), very shallow ($R/a=100$) square cylindrical panel.

in Figure 8 that the second and third natural frequencies are too close to be distinguishable because the panel is very shallow, and behaves more or less like a flat plate. These plots clearly demonstrate the superiority of the mixed type double Fourier series over its single set of double Fourier series counterpart, both in terms of rapidity and monotonicity of convergence. For example, for the fundamental frequency computed using the mixed type double Fourier series, that corresponds to the transverse mode shape, $u_{3(11)}$, the value at $m=n=3$ is within 1·75% of the converged solution. The same is true for the second (equal to the third) natural frequency, corresponding to the transverse mode shape, $u_{3(12)}$ (or $u_{3(21)}$), in which case the mixed series yields a value for $m=n=3$ within 0·3% of the converged solution. The fourth numerically ordered frequency, which corresponds to the

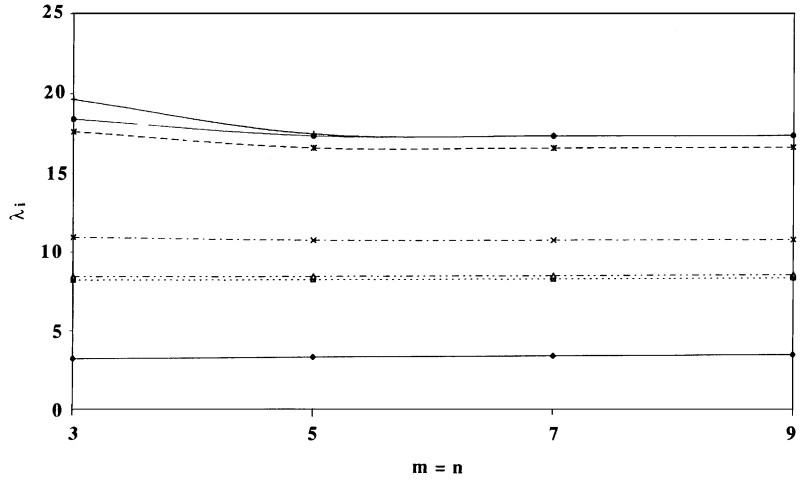

Figure 7. Convergence of seven lowest natural frequencies of a [0°/90°] thin ($a/h=50$), very shallow ($R/a=100$) square cylindrical panel.

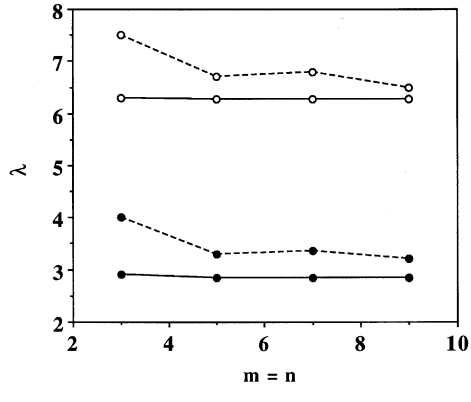

Figure 8. Comparison of the first (●) and second/third (○) natural frequencies computed using the present solution (—) with its single series counterpart (- - -) for a [0°/90°] moderately thick ($a/h=10$), very shallow ($R/a=100$) square cylindrical panel.

inplane mode, $u_{1(11)}$ and/or $u_{2(11)}$, exhibits even more spectacular result in that the convergence is achieved using $m=n=1$. The fifth numerically ordered frequency, corresponding to the transverse mode shape, $u_{3(22)}$, yields a value for $m=n=3$ within 1% of the converged solution. In contrast, the single series solutions for the same frequencies seem almost flat-footed. Although they are able to capture the correct trend, none of them computed using $m=n=3$ is within even 15% of their converged counterparts.

The present results are compared with the available finite element solution [15] in Table 1. These results are presented in order to validate the accuracy of the FEM results. These FEM results could not be validated until now, because no analytical solution to the problem existed in the literature. Getting FEM results are much easier than validating them because of scarcity of available analytical solutions in the literature. A four-node shear-flexible finite element is selected to compare the results with the present solution.

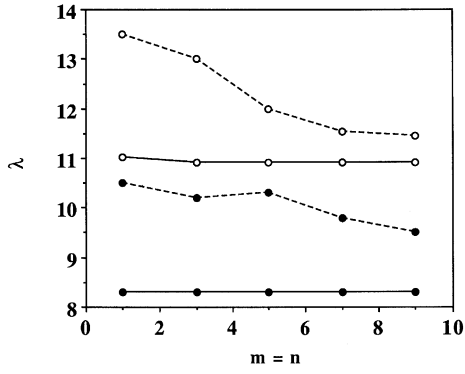

Figure 9. Comparison of the fourth (●) and fifth (○) natural frequencies computed using the present solution (—) with its single series counterpart (—) for a [0°/90°] moderately thick ($a/h = 10$), very shallow ($R/a = 100$) square cylindrical panel.

TABLE 1

Comparison of the present solution with the finite element results [15] for a [0°/90°] moderately thick (a/h=10), very shallow (R/=100) square cylindrical panel

Natural frequency	Present solution
	Finite element solution [15]
1	0·962
2	0·970
3	0·970
4	0·914
5	0·992

Five lowest natural frequencies are compared for a moderately thick ($a/h = 10$) very shallow ($R/a = 100$) panel of square planform ($b/a = 1$). The two sets of results are sufficiently close (within 4%) to validate the accuracy and robustness of the FEM results, and also to lend added credence to the present solution procedure.

Contours depicting the mode shapes (or eigenfunctions) are plotted for moderately thick ($a/h = 10$) and very shallow ($R/a = 100$) panels, and are shown in Figures 10–18. In these plots, $u_{3(mn)}$ denotes the mode shape for transverse vibration with $m = n = 1, 2, 3$ and so on. The mode shapes give important insight into the dynamic response of the anti-symmetric cross-ply [0°/90°] cylindrical panels under investigation. Figures 10–18, which are contour plots, clearly depict the mode shape patterns, $u_{3(11)}$, $u_{3(12)}$, $u_{3(21)}$, $u_{3(22)}$, $u_{3(23)}$, $u_{3(32)}$ and $u_{3(33)}$ respectively. Furthermore, as expected for a very shallow panel, the contour plot pairs, $u_{3(12)}$ and $u_{3(21)}$, and $u_{3(23)}$ and $u_{3(32)}$ exhibit symmetry of patterns, that can be obtained by rotation of $\pm 90°$ from each other, because both transverse mode shapes correspond to the same natural frequency. The same is not true for the contour plots corresponding to the mode shapes, $u_{3(13)}$ and $u_{3(31)}$, shown in Figures 12 and 16, which cannot be obtained by rotation of $\pm 90°$ from each other, although both transverse

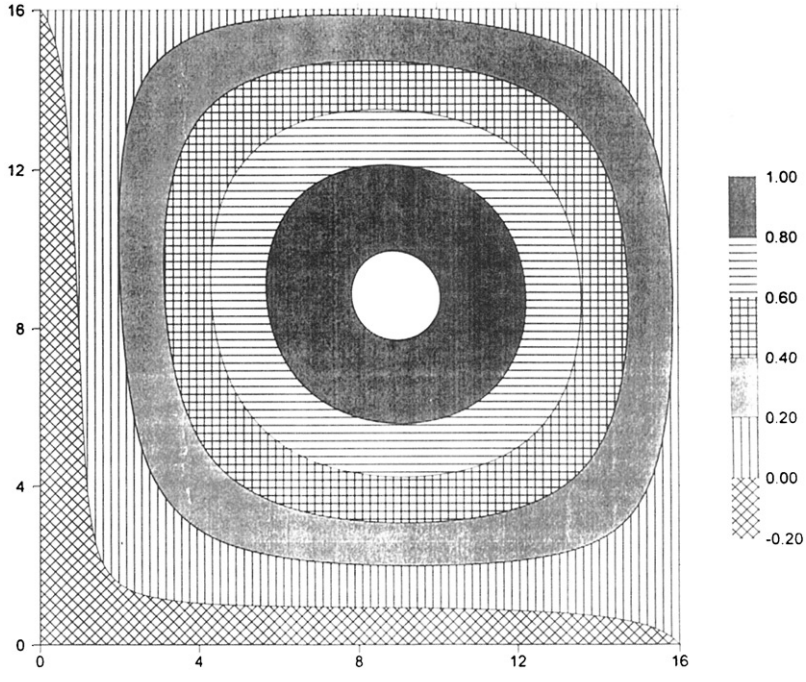

Figure 10. Mode shape, $u_{3(11)}$, for a [0°/90°] moderately thick ($a/h = 10$), very shallow ($R/a = 100$) square cylindrical panel.

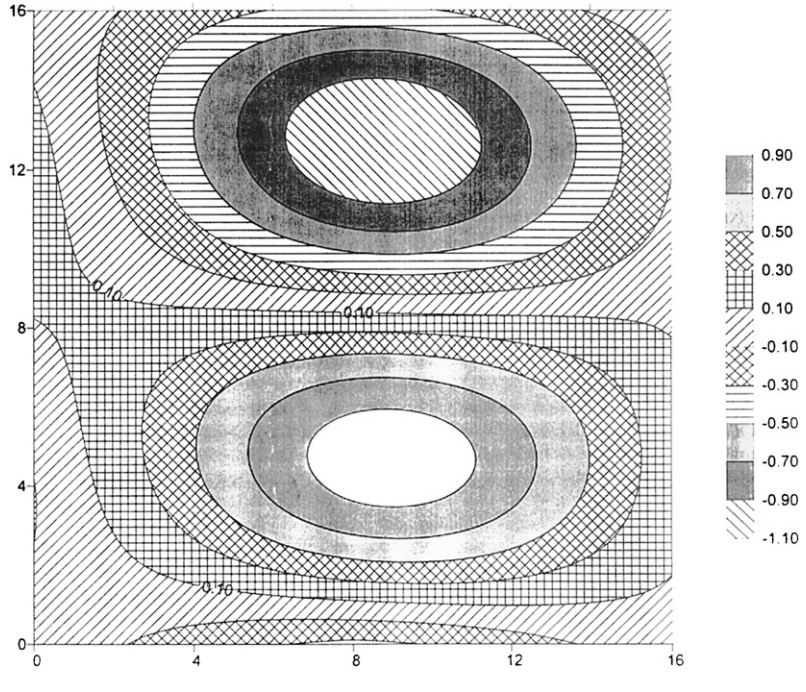

Figure 11. Mode shape, $u_{3(12)}$, for a [0°/90°] moderately thick ($a/h = 10$), very shallow ($R/a = 100$) square cylindrical panel.

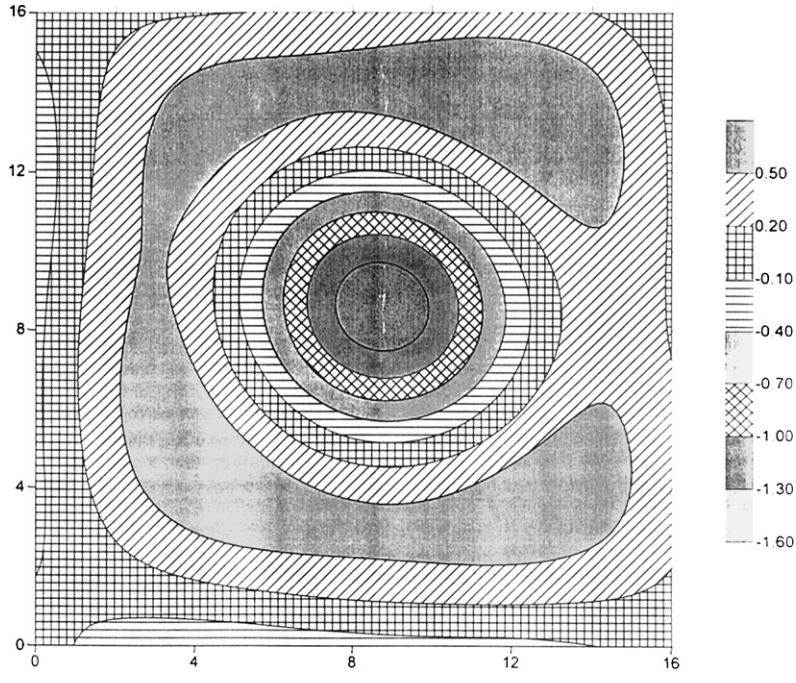

Figure 12. Mode shape, $u_{3(13)}$, for a [0°/90°] moderately thick ($a/h = 10$), very shallow ($R/a = 100$) square cylindrical panel.

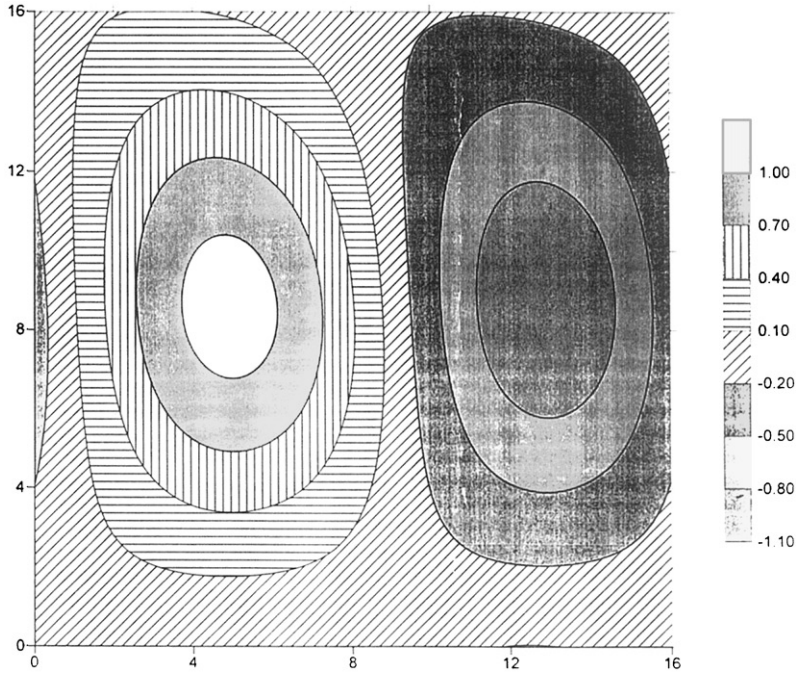

Figure 13. Mode shape, $u_{3(21)}$, for a [0°/90°] moderately thick ($a/h = 10$), very shallow ($R/a = 100$) square cylindrical panel.

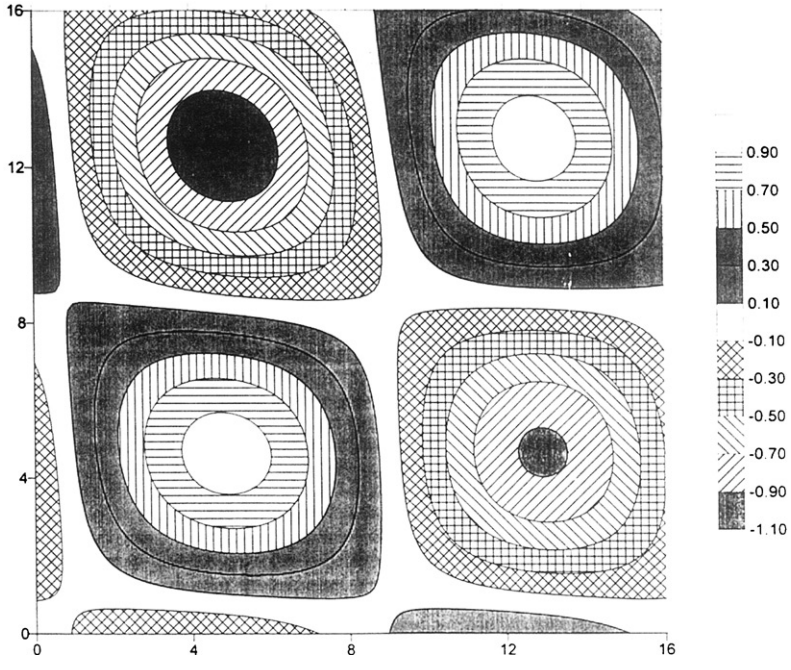

Figure 14. Mode shape, $u_{3(22)}$, for a [0°/90°] moderately thick ($a/h = 10$), very shallow ($R/a = 100$) square cylindrical panel.

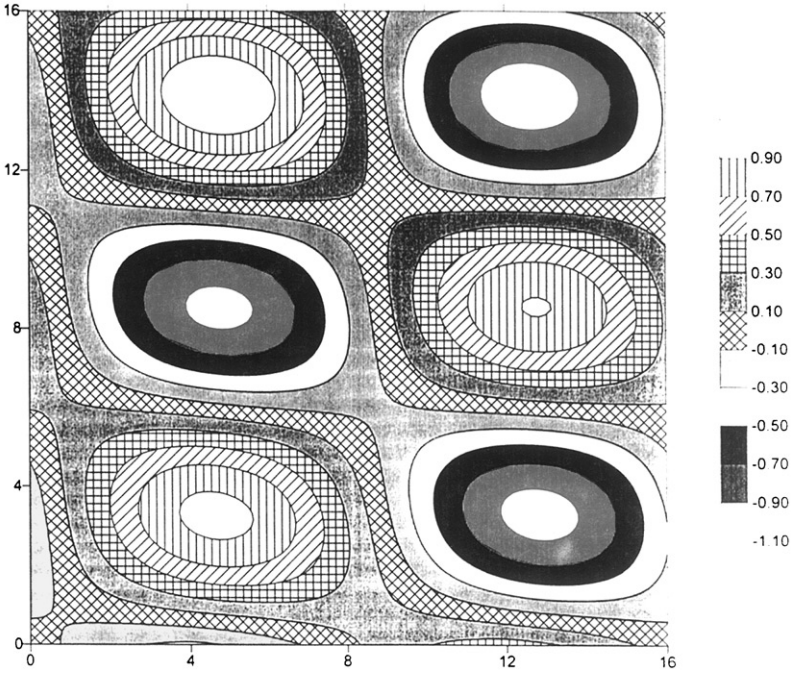

Figure 15. Mode shape, $u_{3(23)}$, for a [0°/90°] moderately thick ($a/h = 10$), very shallow ($R/a = 100$) square cylindrical panel.

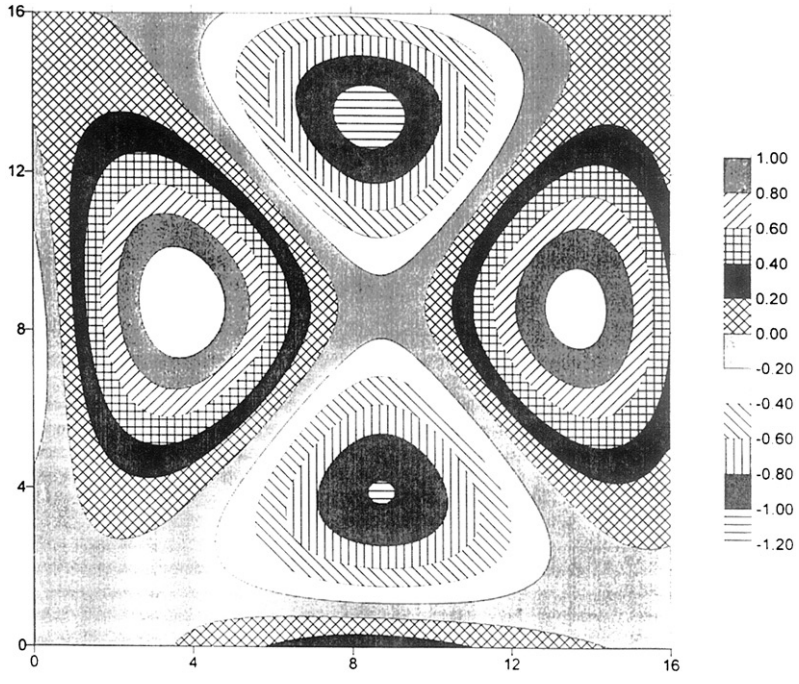

Figure 16. Mode shape, $u_{3(31)}$, for a [0°/90°] moderately thick ($a/h = 10$), very shallow ($R/a = 100$) square cylindrical panel.

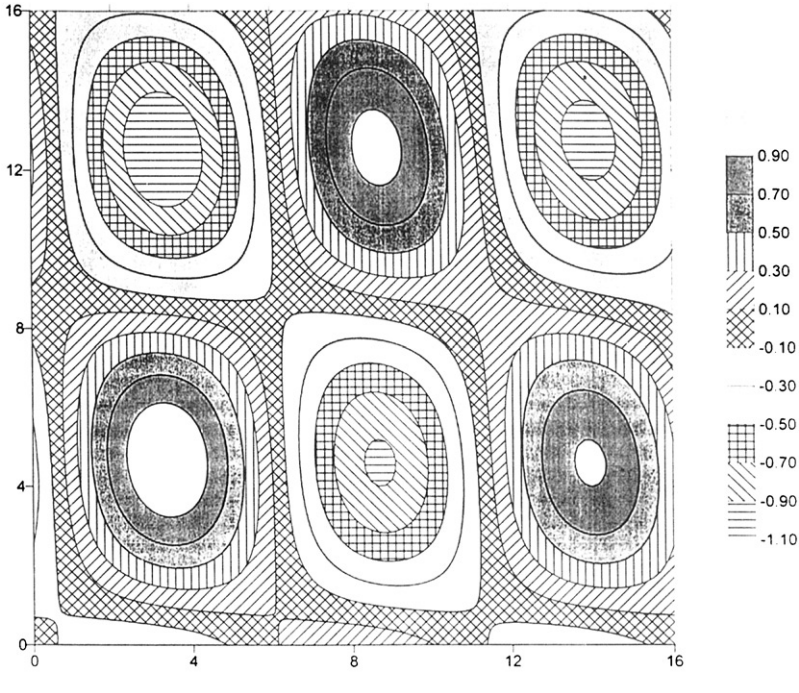

Figure 17. Mode shape, $u_{3(32)}$, for a [0°/90°] moderately thick ($a/h = 10$), very shallow ($R/a = 100$) square cylindrical panel.

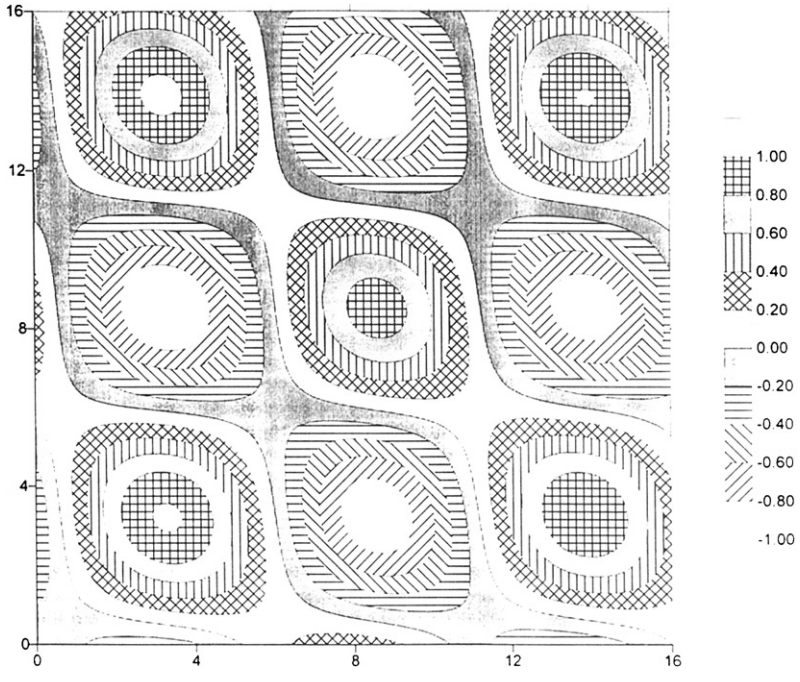

Figure 18. Mode shape, $u_{3(33)}$, for a [0°/90°] moderately thick ($a/h = 10$), very shallow ($R/a = 100$) square cylindrical panel.

mode shapes correspond to the same natural frequency. This is because these contour plots correspond to "degenerate" modes that correspond to the combined action of transverse and surface-parallel modes. For example, Figure 16 clearly exhibits the combined influence of the transverse mode, $u_{3(31)}$ and the surface-parallel shear mode, while Figure 12 depicts the combined effect of the transverse mode, $u_{3(13)}$ and a surface-parallel extensional mode. For thicker panels, as has been shown earlier by Kabir and Chaudhuri [7], surface-parallel modes are expected to play dominant roles except for the fundamental frequency, which corresponds to the transverse mode, $u_{3(11)}$.

Figure 19 exhibits the effect of thickness on the computed seven lowest normalized natural frequencies (eigenvalues) of antisymmetric cross-ply [0°/90°], moderately deep ($R/a = 10$) cylindrical panels of square planform. These natural frequencies generally correspond to the mode shapes, $u_{3(11)}$, $u_{3(12)}$, $u_{3(21)}$, $u_{1(11)}$ (and/or $u_{2(11)}$), $u_{3(22)}$, $u_{3(13)}$, $u_{3(31)}$, although mode switches within the same numerically ordered frequency can be expected, except for the case of the fundamental frequency, with different regimes of the a/h ratio. This has been observed earlier in the case of angle-ply panels [7, 16]. Similar results for very shallow ($R/a = 100$) and virtually flat ($R/a = 1000$) antisymmetric cross-ply [0°/90°] square cylindrical panels are shown in Figures 20 and 21 respectively. The effects of shear deformation, asymmetry of lamination, length-to-thickness ratio and shell curvature on the computed natural frequencies are quite self-evident in these plots. These plots exhibit a highly complex interaction of bending–stretching type coupling effect with those of transverse shear deformation, rotatory inertias, surface-parallel inertias, and membrane action due to shell curvature. These results show that the normalized natural frequencies increase monotonically with the increase of length-to-thickness ratio. One major difference between the dynamic response of a moderately deep shell ($R/a = 10$) shown in Figure 19 and its very shallow counterparts (Figures 20 and 21) is that while in the former all the

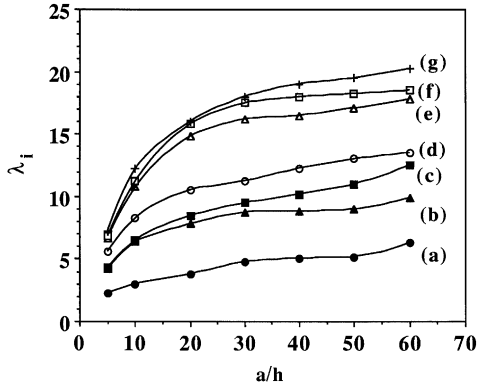

Figure 19. Variation of natural frequencies with the aspect ratio, a/h, of a square, moderately deep ($R/a = 10$) cylindrical panel.

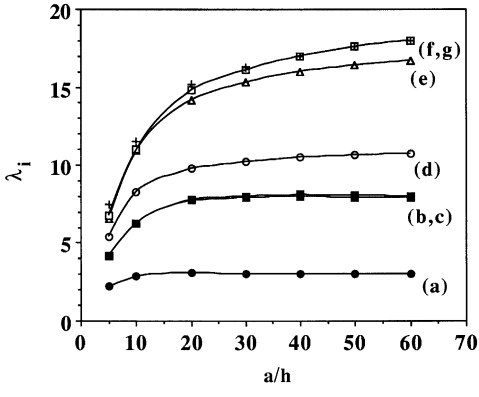

Figure 20. Variation of natural frequencies with the aspect ratio, a/h, of a square, very shallow ($R/a = 100$) cylindrical panel.

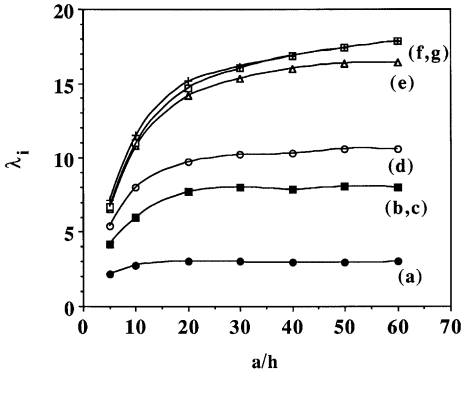

Figure 21. Variation of natural frequencies with the aspect ratio, a/h, of a square, virtually flat ($R/a = 1000$) cylindrical panel.

seven numerically ordered natural frequencies are quite distinct except for very thick panels ($a/h \sim 5$), in the latter the frequencies corresponding to mode shapes, $u_{3(12)}$ (curves b) and $u_{3(13)}$ (curves f) are nearly identical to their counterparts, corresponding to mode shapes, $u_{3(21)}$ (curves c) and $u_3(31)$ (curves g) respectively. It is also noteworthy that the transverse shear deformation, which is generally opposed by the membrane action due to the shell curvature and bending-stretching coupling, dominates in the thicker shell regime, which shows up in the form of steep rises in the λ_i versus a/h curves. For higher frequencies, the region of this dominance extends further into relatively thinner panel regime. As shown in Figure 20 and more so in Figure 21, the lower frequencies of relatively flat panels reach their plateaus at or before $a/h = 40$, which is in line with the behavior of a thin plate. In contrast, the lower frequencies, including the fundamental one, of moderately deep panels display an uncharacteristic rise, albeit a lot less pronounced, even in the very thin panel regime (Figure 19). Unlike in the case of the flatter panels, the membrane action due to shell curvature and surface-parallel inertias, which are, in turn, coupled with rotatory inertias, interact with the bending–stretching coupling to produce such behavior in the thinner moderately deep ($R/a = 10$) panels.

5. CONCLUSIONS

An analytical solution to the problem of an antisymmetric cross-ply cylindrical panel subjected to the SS2 type simply supported boundary condition is presented. Each unknown is expressed in terms of two double Fourier series in which the second set is orthogonal to the first, and represents the error term that may arise out of the presence of discontinuity in the function or it first derivative at the boundary. Although the solution procedure has been illustrated only for a specific shell geometry and lamination and a specific boundary condition, the main idea behind it is general enough to be applicable to any laminated shell problem subjected to any set of admissible boundary conditions.

The convergence characteristics of the computed natural frequencies demonstrate the computational efficiency of the approach. Comparison of the present solution with its single set of double Fourier series counterpart clearly demonstrates the superiority of the mixed type double Fourier series over its rival, both in terms of rapidity and monotonicity of convergence. Furthermore, comparison with available finite element solution not only establishes the accuracy of the latter results, but also lends confidence to the present solution.

The computed natural frequencies (eigenvalues) and mode shapes (eigenfunctions) give important insight into the dynamic response of the cross-ply [0°/90°] cylindrical panels under investigation. These results shed light on the highly complex interaction among the effects of transverse shear deformation, bending–stretching type coupling, membrane action due to shell curvature, rotatory inertias, surface-parallel inertias, etc. in the case of antisymmetric crossply cylindrical panels. The numerical results thus presented can be capitalized as bench-mark solutions for the future comparisons with approximate or weak (integral) forms of solutions, such as finite elements and boundary elements (in the context of FSDT). Extension to such other shell geometry as spherical panel and other boundary conditions and laminations is currently under way, and will be published in a future paper.

ACKNOWLEDGMENTS

This project was funded by the Kuwait University through an agreement number EV106 to the first and second authors. This support is gratefully acknowledged. The authors also

wish to thank the editor and two anonymous reviewers for important suggestions on the original manuscript, which have helped improve the overall quality of the paper.

REFERENCES

1. C. W. Bert and P. H. Francis 1974 *American Institute of Aeronautics and Astronautics Journal* **12**, 1173–1186. Composite material mechanics: structural mechanics.
2. R. A. Chaudhuri 1989 *International Journal of Engineering Science* **27**, 1005–1022. On boundary-discontinuous double Fourier series solution to a system of completely coupled P.D.E.s.
3. C. W. Bert and M. Kumar 1982 *Journal of Sound and Vibration* **81**, 107–121. Vibrations of cylindrical shells of bimodulus composite materials.
4. R. A. Chaudhuri and K. R. Abu-Arja 1988 *International Journal of Engineering Science* **26**, 587–604. Exact solution of shear-flexible doubly curved anti-symmetric angle-ply shells.
5. L. Librescu, A. A. Khdeir and D. Frederick 1989 *Acta Mechnica* **76**, 1–33. A shear deformable theory of laminated composite shallow shell-type panels and their response analysis I, free vibration and buckling.
6. R. A. Chaudhuri and K. R. Abu-Arja 1991 *International Journal of Solids and Structures* **28**, 1–16. Static analysis of moderately thick anti-symmetric angle-ply cylindrical panels and shells.
7. H. R. H. Kabir and R. A. Chaudhuri 1991 *International Journal of Solids and Structures* **28**, 17–32. Free vibrations of anti-symmetric angle-ply finite doubly curved shells.
8. R. A. Chaudhuri and H. R. H. Kabir 1992 *International Journal of Solids and Structures* **30**, 263–272; 273–286. Sensitivity of the response of moderately thick cross-ply doubly-curved panels to lamination and boundary constraint. Part-I: theory, Part-II: application.
9. H. R. H. Kabir and R. A. Chaudhuri 1994 *International Journal of Engineering Science* **32**, 501–520. On Gibbs-phenomenon-free Fourier solution for finite shear-flexible laminated clamped curved panels.
10. R. A. Chaudhuri and H. R. H. Kabir 1994 *Composite Structures* **28**, 73–91. Static and dynamic analysis of finite general cross-ply doubly curved panels using classical shallow shell theories.
11. R. A. Chaudhuri and H. R. H. Kabir 1995 *American Institute of Aeronautics and Astronautics Journal* **33**, 1681–1688. Fourier solution to higher-order theory based laminated shell boundary-value problem.
12. Y. A. Melnikov 1995 *Green's Functions in Applied Mechanics*. Boston: Computational Mechanics Publications.
13. J. L. Sanders Jr 1959 An Improved First-Approximation Theory for Thin Shells. *NASA Technical Report*, *R*-24.
14. *IMSL Manual*. CA, 1992.
15. *NISA-II Manual*. MI, Troy, 1997.
16. R. A. Chaudhuri and H. R. H. Kabir 1992 *International Journal of Engineering Science* **30**, 1647–1664. A boundary-continuous-displacement based Fourier analysis of laminated doubly-curved panels using classical shallow shell theories.